Phase Diagram Cuspidine ($3CaO \cdot 2SiO_2 \cdot CaF_2$)-$CaF_2$

TAKASHI WATANABE, HIROYUKI FUKUYAMA, MASAHIRO SUSA, and KAZUHIRO NAGATA

Equilibrium phase diagram for the system cuspidine ($3CaO \cdot 2SiO_2 \cdot CaF_2$)-$CaF_2$ has been studied by the quenching method and differential thermal analysis (DTA). Hermetically closed platinum capsules were used in both methods to prevent fluorine loss in the form of HF and SiF_4 by reaction of the CaF_2 with water vapor or SiO_2. Cuspidine congruently melts at 1680 ± 2 K. The cuspidine-CaF_2 system presents a simple eutectic type of phase diagram. The eutectic composition and temperature are 46 mass pct $3CaO \cdot 2SiO_2$ − 54 mass pct CaF_2 and 1515 ± 3 K, respectively.

I. INTRODUCTION

FURTHER development in mold flux for the continuous casting of steel is indispensable to improve the casting rate and quality of products. Mold flux plays considerably important roles in the continuous casting process. The main roles are (1) lubrication between strand and mold, (2) heat transfer from strand to mold, (3) thermal insulation on the top surface of the molten pool, (4) protection of the steel from reoxidation, and (5) absorption of inclusions on the surface of strand. All of them have a decisive effect on the quality of the products.

For instance, nonuniform cooling of strand caused by partial crystallization of mold flux brings about the surface defects of slab due to thermal stress.[1] In particular, a ternary compound, cuspidine ($3CaO \cdot 2SiO_2 \cdot CaF_2$), crystallizes in various kinds of flux films during the casting,[2] and the crystallization affects the heat transfer.[3] Therefore, it is very important to control the crystallization of cuspidine for the optimal continuous casting process. From this point of view, isothermal transformation diagrams (so called TTT diagram)[4,5] and continuous cooling transformation diagrams (CCT diagram)[6] have been studied on mold fluxes. However, very little work is currently available in the published literature on the fundamental physicochemical data of mold flux, such as phase diagrams and Gibbs energies of formation of compounds crystallized in mold fluxes. Thus, the present authors have focused on the CaO-SiO_2-CaF_2 ternary system based on the current mold flux constituents.

Mukerji reported the phase diagram for the CaO-$2CaO \cdot SiO_2$-CaF_2 system in 1965,[7] and Hillert proposed the phase diagram for the CaO-SiO_2-CaF_2 system in 1966 by combining his data with Mukerji's results.[8] However, cuspidine was not identified in their studies.[7,8] Only the solid phase equilibria including cuspidine in the CaO-SiO_2-CaF_2 ternary system at 1173 K are currently available, which were reported by Brisi in 1957.[9] The present authors have already successfully synthesized cuspidine and compared the X-ray diffraction profile with those of the natural and synthetic cuspidines, recognizing cuspidine as a thermodynamically stable phase in the system.[10,11] Thus, the ternary phase diagram has not been clearly understood yet because of the experimental difficulties in studying a system containing CaF_2.

The aim of this study is to experimentally determine the equilibrium phase diagram of the cuspidine-CaF_2 system by employing the quenching method and differential thermal analysis (DTA), which is the first step to establish the entire CaO-SiO_2-CaF_2 ternary system. In both methods, samples were hermetically sealed in platinum containers to completely prevent fluorine loss in the form of HF and SiF_4 by reaction of the CaF_2 with water vapor or SiO_2, which led to reproducible results.

II. EXPERIMENTAL

A. *Sample Preparation*

Reagent grade powders of $CaCO_3$ (99.5 mass pct), SiO_2 (99.9 mass pct), and CaF_2 (99.95 mass pct) were used as initial samples.

1. *Rankinite ($3CaO \cdot 2SiO_2$)*

Rankinite was synthesized by mixing powders of $CaCO_3$ and SiO_2 at the molar ratio of $CaCO_3 : SiO_2 = 3 : 2$. The powders were pressed in a tablet and sintered in air at 1673 K for 259.2 ks (3 days). The tablets were quenched, ground, pressed again, and resintered at 1673 K for 259.2 ks (3 days) to completely form rankinite. The obtained samples were identified as rankinite with no other phase by X-ray diffractometry (XRD).

2. *Cuspidine ($3CaO \cdot 2SiO_2 \cdot CaF_2$)*

Stoichiometric cuspidine has a molar ratio of $CaO : SiO_2 : CaF_2 = 3 : 2 : 1$. Cuspidine was synthetically prepared by mixing equimole of rankinite and CaF_2. During the synthesis, samples should be isolated from moisture at elevated temperatures, because samples containing CaF_2 react with water vapor and liberate hydrogen fluoride gas (HF) as follows:

$$CaF_2\ (s) + H_2O\ (g) = CaO\ (s) + 2HF\ (g) \qquad [1]$$

resulting in a change in initial compositions. Cuspidine also reacts with water vapor and forms dicalcium silicate as follows:[9]

$$3CaO \cdot 2SiO_2 \cdot CaF_2\ (s) + H_2O\ (g) = 2(2CaO \cdot SiO_2)\ (s) + 2HF\ (g) \qquad [2]$$

Therefore, to prevent this reaction, the mixed powder of

TAKASHI WATANABE, Graduate Student, HIROYUKI FUKUYAMA, Associate Professor, and KAZUHIRO NAGATA, Professor, Department of Chemistry and Materials Science, and MASAHIRO SUSA, Associate Professor, Department of Metallurgy and Ceramics Science, are with the Tokyo Institute of Technology, Tokyo 152-8552, Japan

Manuscript submitted January 18, 2000.

Table I. Initial Compositions of the Samples Studied in Mass Percent

Sample	Mass Pct $3CaO \cdot 2SiO_2$	Mass Pct CaF_2
1	71.98	28.02
2	70.84	29.16
3	63.50	36.50
4	55.14	44.86
5	51.25	48.75
6	50.00	50.00
7	40.00	60.00
8	30.00	70.00
9	18.88	81.12
10	10.00	90.00

rankinite and CaF_2 was annealed under dried air atmosphere at 1473 K for 36 ks (10 hours). The formation of the cuspidine single phase was confirmed by XRD.

B. *Phase Equilibria in the Cuspidine-CaF_2 System*

Powders of the synthetic rankinite and CaF_2 were mixed at various ratios, as presented in Table I. The powders were hermetically sealed in platinum pipes (o.d. 4 mm × o.d. 3.8 mm × 25 mm) to completely prevent the reaction of CaF_2 with water vapor. Furthermore, dried air or argon was passed through a reaction tube at a flow rate of 20 mL/min during the experimental runs. The sample in the platinum container was hung in a uniform temperature region in a SiC resistance furnace. In order to promote reactions, the samples were first kept at 1708 K for 10.8 ks (3 hours), which was higher than the experimental temperature by 35 to 250 K. Subsequently, the temperature was gradually decreased to the experimental temperatures at a rate of 1 K/min and the samples were held for 20.9 ks (5.8 hours) to 259.2 ks (72 hours) to attain an equilibrium, followed by water quenching. Quenched samples were identified by XRD and electron probe microanalysis (EPMA). Even employing water quenching, crystallization of liquid occurred very easily in the system. Therefore, when the liquidus compositions were quantitatively analyzed by EPMA, a large analytical area was taken to obtain average liquidus compositions. Amorphous SiO_2, single crystalline CaF_2, and synthetic dense cuspidine were used as standard samples in the quantitative analysis. In addition, the experimental difficulty in quantitative analysis of fluorine by EPMA was coped with the help of DTA.

Platinum containers were sometimes chemically attacked in case of CaF_2-rich samples and long-time and high-temperature experiments. Only fine samples were used in this study.

C. *DTA in the Cuspidine-CaF_2 System*

Figure 1(a) shows the experimental setup for DTA, which was performed by using a vertically mounted image furnace of infrared radiation. An alumina cap coated with a platinum foil was covered on samples to obtain a large uniform temperature region. Temperature was controlled within ±0.2 K using a PID controller. A sample holder has been developed to prevent the reaction of CaF_2 with water vapor. A sample was held in a platinum holder, which was made from platinum tubing (o.d. 4 mm × o.d. 3.8 mm × 15 mm), as shown in Figure 1(b). Both ends of the platinum tube were

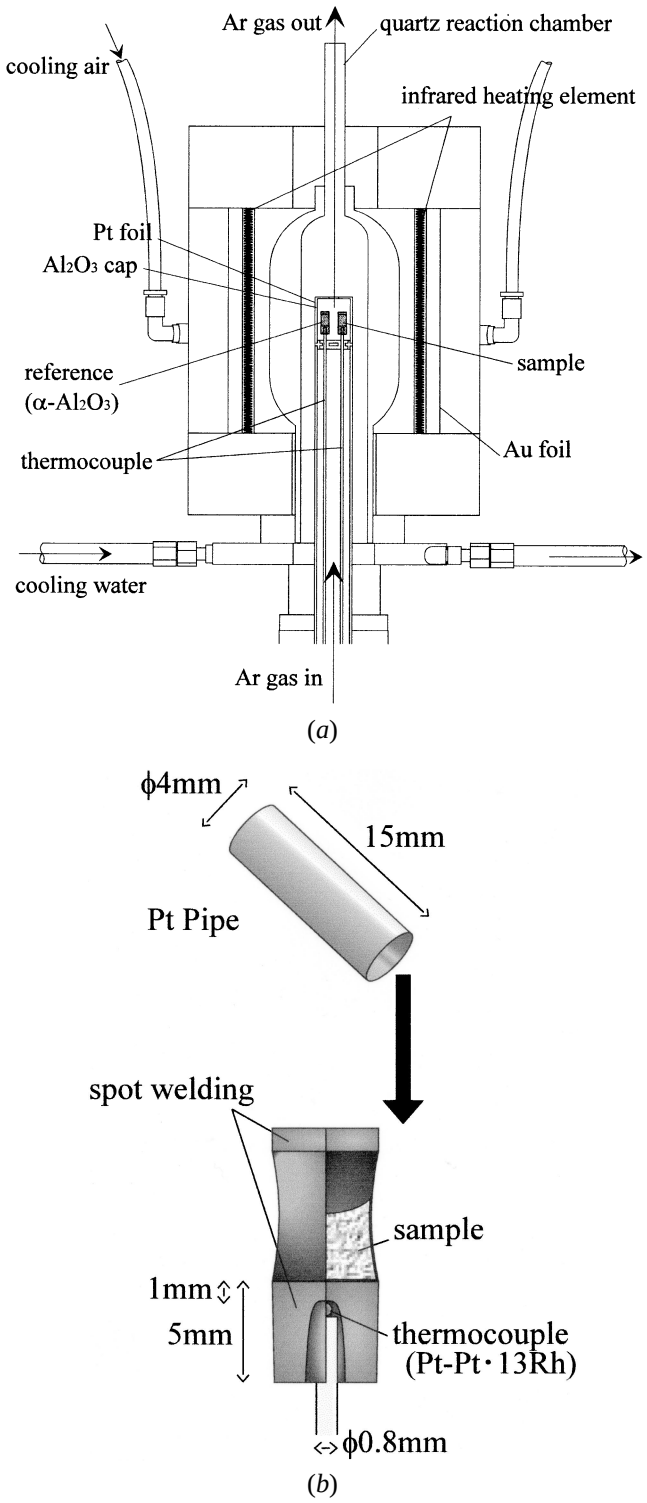

Fig. 1—Schematic diagram of (*a*) apparatus for DTA and (*b*) platinum-sealed sample holder.

hermetically welded to isolate sample and a thermocouple was inserted from the bottom to rest below weld. The same hermetic platinum holder was used for a reference holder to satisfy the identical condition with the sample holder. α-alumina was used as a reference material. Argon gas (99.9999 vol pct) was passed through the reaction chamber at a flow rate of 50 mL/min during DTA. A thermocouple was calibrated using the melting points of MgF_2 and CaF_2

in a temperature range of 1521 to 1695 K. Single crystalline MgF_2 (99.99 mass pct) and CaF_2 (99.994 mass pct) were used, and these melting points are reported as 1521[12] and 1695 K,[13,14] respectively. Kojima and Masson[15] reported the value of 1696 ± 1.5 K as a melting point for pure CaF_2, while Suito and Gaskell[14] reported the value of 1695 ± 0.3 K using the same experimental method with Kojima and Masson. Taking into account that these two data are in good agreement with each other within an experimental uncertainty and the data provided by Suito and Gaskell have given a smaller uncertainty, the melting point of 1695 K has been adopted in the present study. Weighed powders of CaO, CaF_2, and SiO_2 were mixed to give various initial compositions in the cuspidine-CaF_2 system, as shown in Table I.

Prior to the measurements, each sample was first melted by heating to 1723 K at a rate of 5 K/min, and subsequently cooled to room temperature at 50 K/min to standardize initial conditions. The DTA results obtained on heating were taken as data because of the occurrence of supercooling on cooling. In general, a higher heating rate increases the peak height of DTA curves, whereas a lower rate yields higher resolution. Therefore, the heating rate was varied from 1 to 10 K/min to obtain extrapolated values at 0 K/min. Thus, the melting point of cuspidine and the eutectic temperature in the system were determined by the extrapolation method. However, the peaks corresponding to the liquidus temperatures were too small to decide the peak position in the case of slow heating rates; therefore, the values obtained for the heating rate of 5 K/min were used. In both cases, calibration was conducted using a relation between the melting points of CaF_2 and MgF_2 and the peak temperatures obtained by the respective procedures. The details are explained in Section III.

Mass change of samples during the course of DTA was negligible, taking into account weight loss of platinum capsules by evaporation. This means that the initial compositions of samples did not change during DTA.

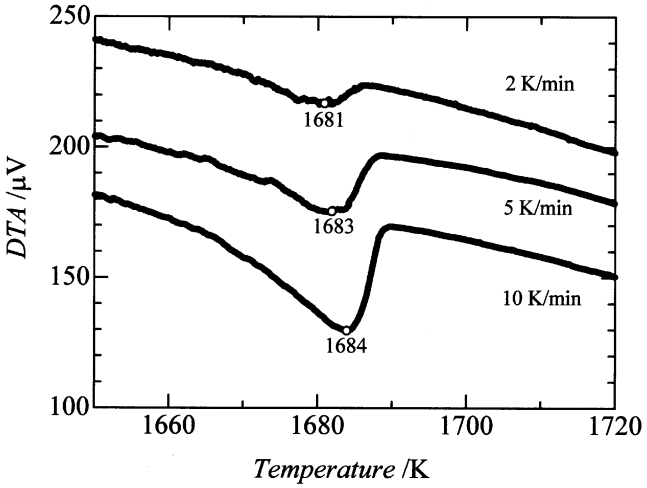

(*a*)

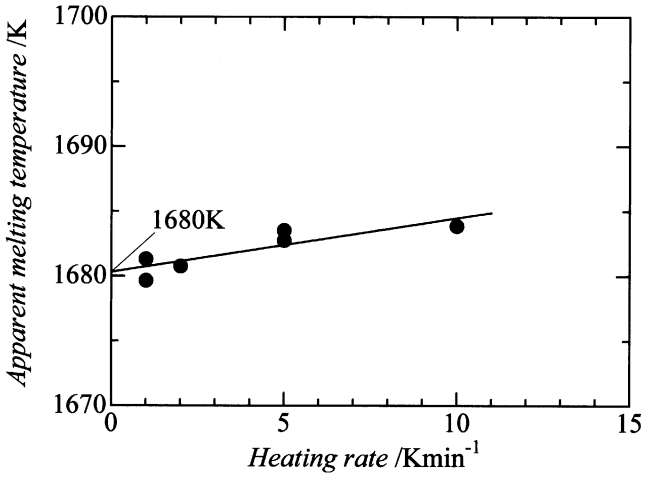

(*b*)

Fig. 2—(*a*) DTA of cuspidine at heating rates of 2, 5, and 10 K/min. (*b*) Determination of the melting point of cuspidine by extrapolating to the value at 0 K/min by least-squares fitting.

III. RESULTS

A. *Melting Point of Cuspidine by DTA*

Figure 2(a) shows the DTA curves of cuspidine with various heating rates, 10, 5, and 2 K/min. Endothermic peaks are observed on melting cuspidine. The peak height and area become larger and the peak position slightly shifts toward higher temperature with increasing heating rate. In the present study, the melting point of cuspidine is determined by the following procedure from the DTA curves.

In general, there are three points to determine a transition temperature, *i.e.*, (1) a start of the peak, (2) an extrapolated onset, and (3) a peak temperature as schematically presented in Figure 3(a).[16] If DTA measurements are conducted with ideal conditions, *i.e.*, heat capacity of a sample is very small and thermal conductivity of a sample is very large, these three points would be identical, as illustrated in Figure 3(b). In addition, these three points converge on a true transformation temperature at a heating rate of 0 K/min by extrapolation, as schematically shown in Figure 3(c). Thus, selection of methods depends on nature of samples

As shown in Figure 2(a), it is difficult to determine the melting point using (1) the start of a peak or (2) an extrapolated onset due to the mild peak shape. Therefore, (3) the peak temperature is chosen as the apparent melting point. By using this point, experimental errors caused by human bias can be minimized, and a good reproducibility was obtained. Figure 2(b) shows the heating-rate dependence of the apparent melting point of cuspidine. The apparent melting point linearly decreases with a decrease in heating rate. All of the data points were subjected to least-squares fitting. The melting point of cuspidine is determined as 1680 ± 2 K by extrapolating to the value at 0 K/min.

No peak appeared in the DTA curves after passing the melting point of cuspidine, as shown in Figure 2(a). In addition, no crystalline phase existed except for cuspidine detected by XRD in air-quenched samples from 1723 K. These facts indicate that cuspidine melts congruently.

B. *Phase Equilibria by Quenching Method*

1. *Two-phase region of cuspidine plus liquid*

Figure 4(a) shows the X-ray images of silicon and fluorine of sample S3-1573-20 quenched after annealing at 1573 K for 72 ks (20 hours). Two different phases containing silicon are observed. One is identified as a primary cuspidine phase

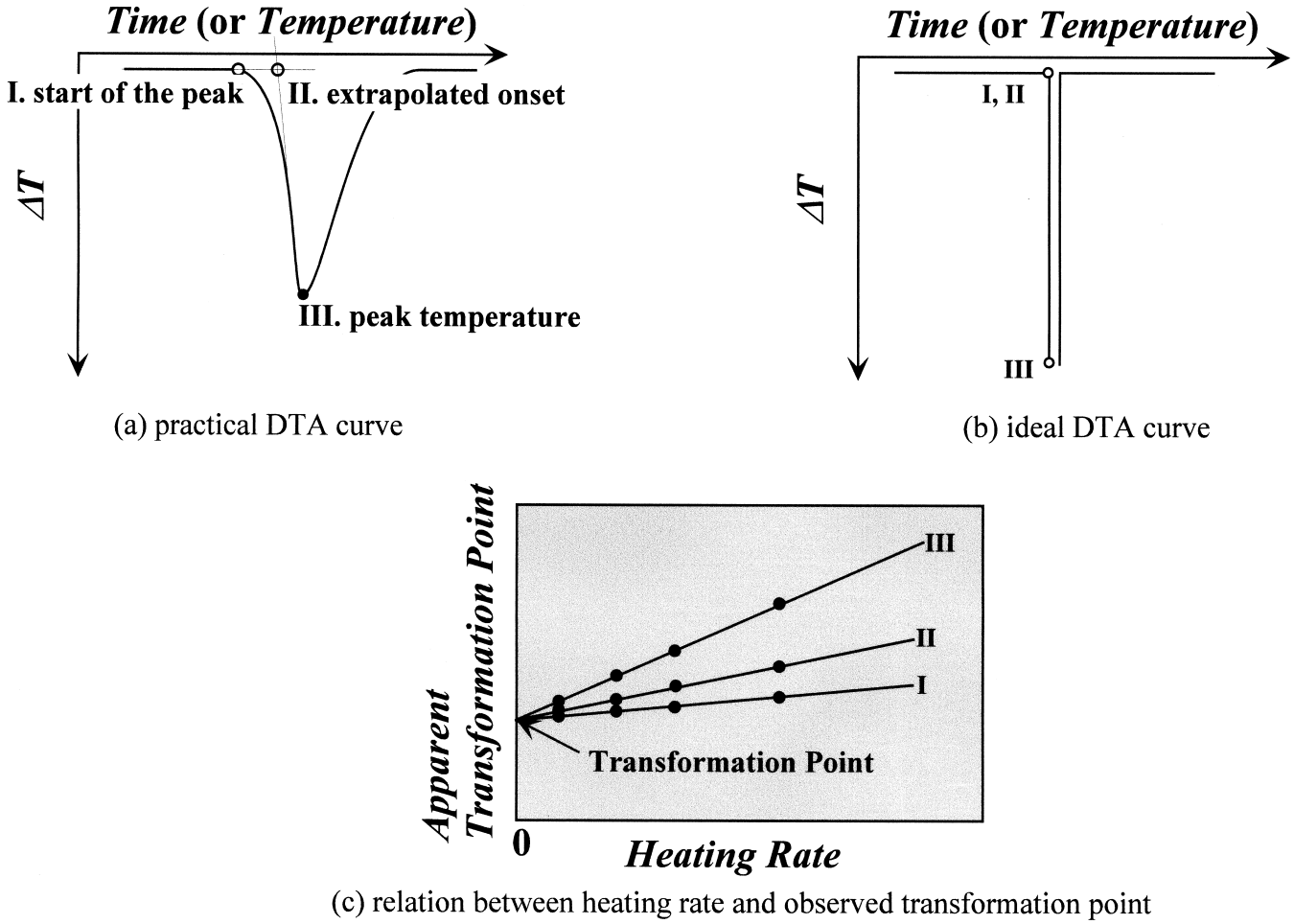

Fig. 3—(*a*) through (*c*) Determining method of transformation temperature in the DTA.

by EPMA quantitative analysis and XRD. From the XRD profile shown in Figure 5(a), the strong peaks for cuspidine are detected, and weak and broad peaks for CaF_2 also appeared. The detected CaF_2 was secondarily precipitated from liquid by the eutectic reaction

$$\text{liquid} \rightarrow \text{cuspidine} + CaF_2$$

during the quenching process. This eutectic microstructure gradually grew toward the center of the sample because of delay in cooling. Even though the water quenching method with small platinum capsules was used, it is still difficult to suppress the crystallization of the liquid phase in the present system. Thus, not only XRD results but also microstructure observation should be required to reveal the phase equilibria. The formed microsegregation causes errors in EPMA quantitative analysis for liquid phases; therefore, a large analysis area was taken to minimize scattering in results.

To confirm whether an equilibrium was reached, time dependence of the liquidus compositions was studied for the samples of S3-1573-5.8, S3-1573-20, and S3-1573-72 and is shown in Figure 6. The error bars correspond to the experimental uncertainty due to microsegregation. This figure shows that the sample reached an equilibrium in 20.9 ks (5.8 hours). Table II summarizes the experimental conditions and the equilibrium phases observed in samples and the liquidus compositions for all of the quenching experiments. In some samples, very weak XRD peaks of $2CaO \cdot SiO_2$ appeared, because the chemical composition slightly deviated from the cuspidine-CaF_2 binary and moved into the three-phase region of cuspidine-$2CaO \cdot SiO_2$-CaF_2.

Solubility of CaF_2 in the primary cuspidine phase is negligible from the EPMA quantitative analysis.

2. *Two-phase region of CaF_2 plus liquid*

Figures 4(b) and 5(b) show the X-ray images of silicon and fluorine and the XRD profile for sample S9-1573-72 annealed at 1573 K for 259.2 ks (72 hours), respectively. From these figures, it is found that solid CaF_2 equilibrated with the corresponding liquid at 1573 K. Weak and broad XRD peaks of cuspidine are due to the secondary precipitation from the liquid during quenching process by the rapid eutectic reaction

$$\text{liquid} \rightarrow \text{cuspidine} + CaF_2$$

To estimate solubility of cuspidine in primary CaF_2 phase, silicon content in CaF_2 phase was analyzed by EPMA using cuspidine and SiO_2 as standard samples. The CaF_2 phase contains 0.01 mass pct of silicon, corresponding to 0.25 mass pct of cuspidine at 1623 K.

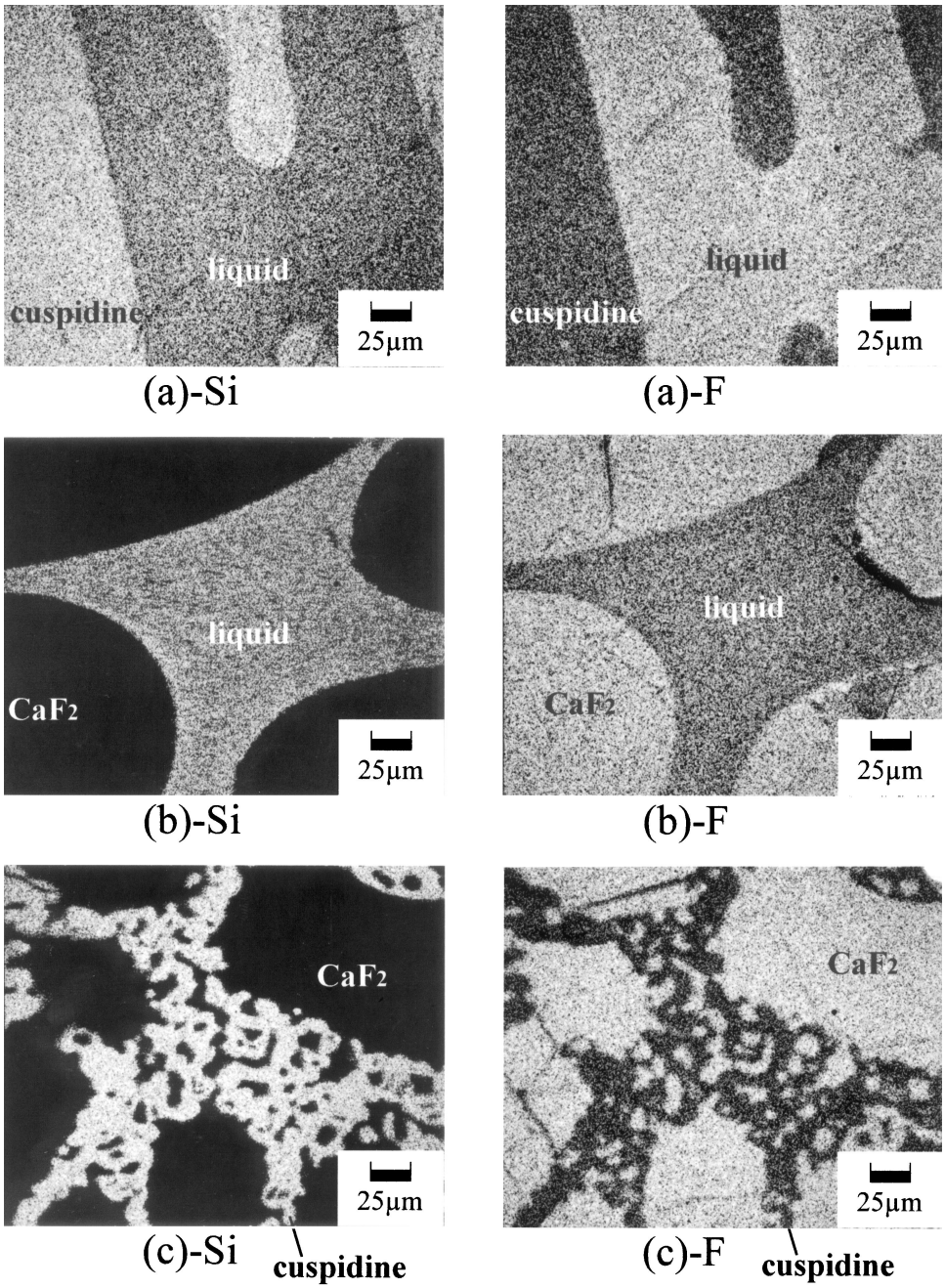

Fig. 4—X-ray image of silicon and fluorine of the samples: (*a*) cuspidine + liquid (S3-1573-20), (*b*) CaF_2 + liquid (S9-1573-72), and (*c*) eutectic structure (S9-1473-72).

3. *Eutectic structure of cuspidine and CaF_2*

Figure 4(c) shows the X-ray images of silicon and fluorine of sample S9-1473-72 annealed at 1473 K for 259 ks (72 hours). Large grains of CaF_2 are observed, which grew in the primary crystallization field of CaF_2 during the course of slow cooling from 1708 K to the experimental temperature, 1473 K. The other part is the eutectic structure consisting of cuspidine and CaF_2, which developed during annealing at 1473 K. Figure 5(c) shows the XRD profiles of the sample, which demonstrates that CaF_2 and cuspidine exist in the sample. Thus, CaF_2 equilibrate with cuspidine in a solid state at 1473 K, which is below the eutectic temperature.

C. *DTA in the Cuspidine-CaF_2 System*

Figure 7 shows a typical DTA curve of sample 9 for the temperature range from 1200 to 1700 K. The first large peak indicates the eutectic temperature and the second one corresponds to the liquidus temperature. When the sample reaches the eutectic temperature on heating, a liquid phase forms by the eutectic reaction, and a large endothermic peak

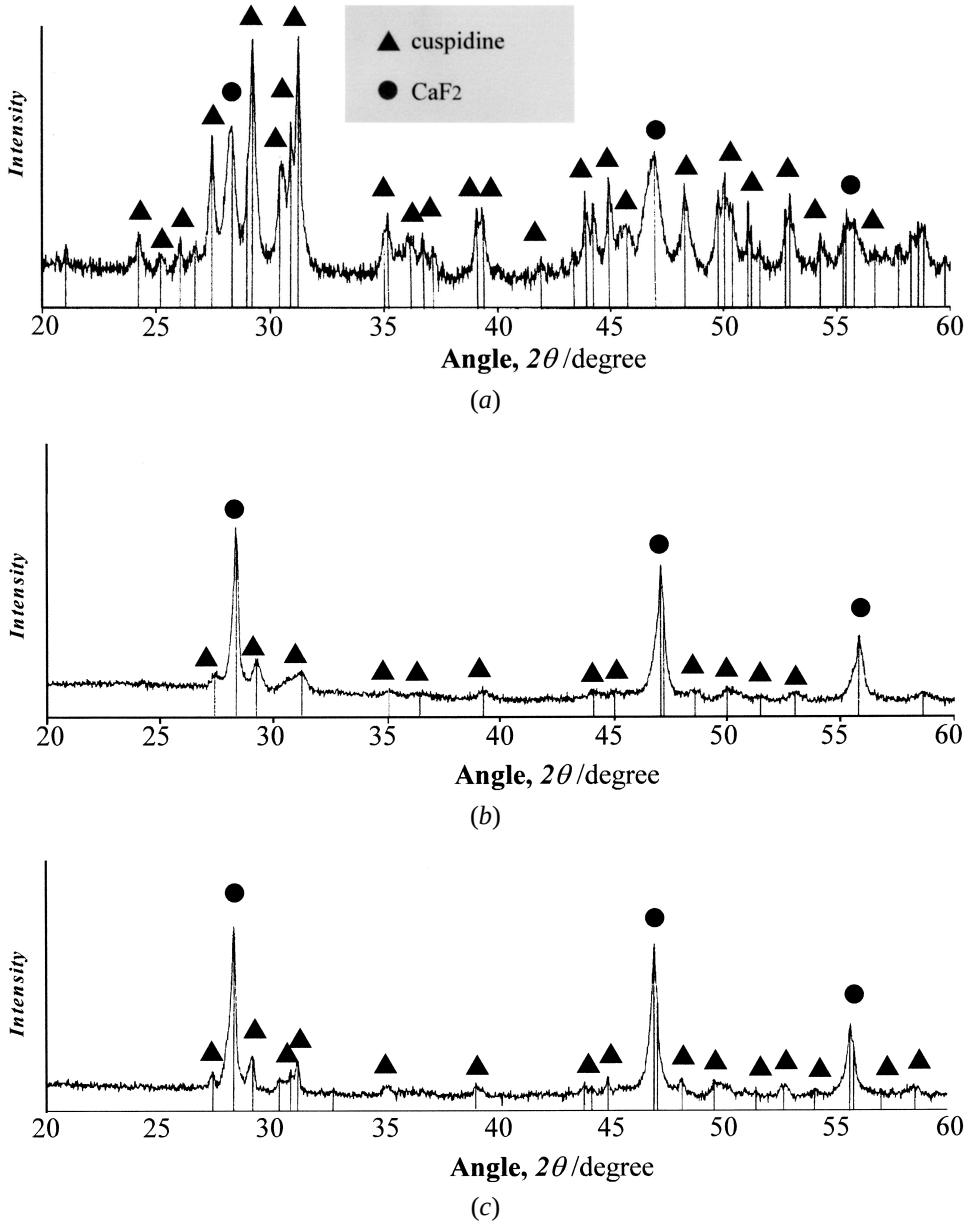

Fig. 5—XRD profiles of the samples: (*a*) cuspidine + liquid (S3-1573-20), (*b*) CaF_2 + liquid (S9-1573-72), and (*c*) cuspidine + CaF_2 (S9-1473-72).

appears. Subsequently, a small peak appears at the liquidus temperature. The true eutectic temperatures were determined by extrapolating to the value of 0 K/min, while the liquidus temperatures obtained for the heating rate of 5 K/min were used as explained in Section II. Table III summarizes the DTA results.

After the DTA measurement, the sample was subjected to EPMA. Figure 8(a) shows the X-ray image of silicon of sample 9, and the enclosed area in (a) is enlarged in (b). The primary crystal of CaF_2 and the eutectic structure of cuspidine and CaF_2 are observed.

IV. DISCUSSION

A. *Melting Point of Cuspidine*

The present authors previously reported that the melting point of cuspidine is 1684 ± 1 K by the measurement of the apparent electric resistance of cuspidine.[10] In the previous report, the sharp increase in the electric resistance observed was considered to relate to the fusion of cuspidine. However, it was a rather indirect measurement compared with DTA, because the sharp change in the resistance depended highly on the mechanical contact between a lead wire and cuspidine powder in the hermetic sample container. Therefore, the authors believe that the present result obtained by DTA is more reliable. Valkenburg and Rynders reported that the melting point of synthetic cuspidine was determined to be 1683 ± 10 K by the quench technique.[11] The present data obtained agree with their data within a reasonable experimental error.

B. *Phase Diagram of the Cuspidine-CaF_2 System*

Figure 9 shows the phase diagram of the cuspidine-CaF_2 system constructed based on the all results measured by both

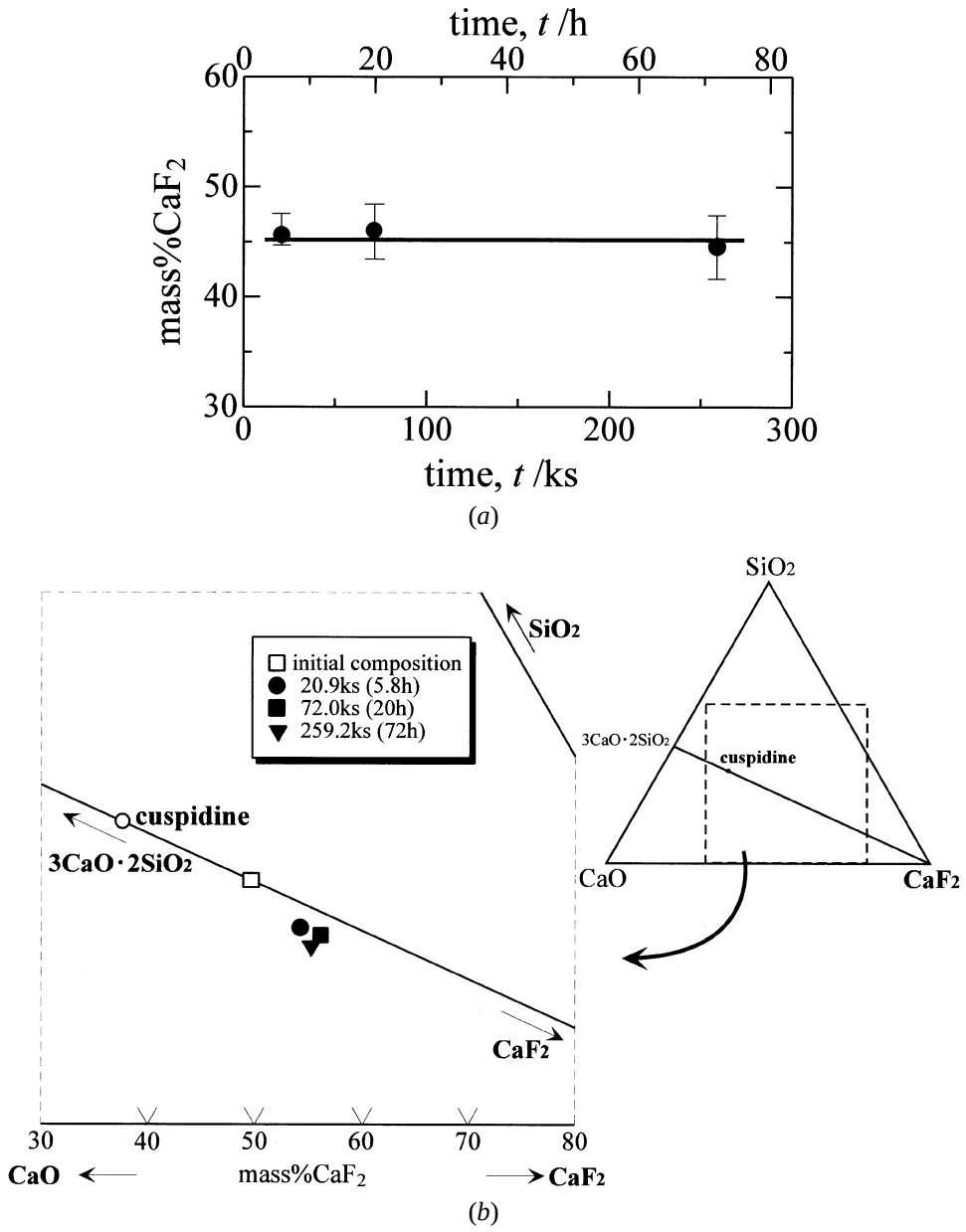

Fig. 6—(*a*) Time dependence of the liquidus compositions for sample 3 of S3-1573-5.8, S3-1573-20, and S3-1573-72. (*b*) The liquidus compositions plotted in the partial phase diagram of the CaO-SiO_2-CaF_2 system.

the quenching method and DTA. Half-filled and filled circles denote the initial compositions of the samples annealed in the two-phase regions of (cuspidine plus liquid), (CaF_2 plus liquid), and (cuspidine plus CaF_2), respectively, obtained by the quenching experiments. Open circles with error bars express the corresponding liquidus compositions measured by EPMA. Open squares express the initial composition of the samples, which are in a homogeneous liquid region. On the other hand, two kinds of filled triangles express the liquidus and eutectic temperatures obtained by DTA. The eutectic temperature and composition are determined as 1515 ± 3 K and 46 mass pct 3CaO · 2SiOi2 − 54 mass pct CaF_2, respectively. The liquidus lines are drawn by relying more preferentially on the DTA results than on the results obtained by the quenching methods, because the quantitative analysis of fluorine by EPMA contains a relatively large experimental uncertainty.

C. *Comparison with Hillert's Result on the Ternary Phase Diagram of the CaO-SiO_2-CaF_2 System*

Hillert[8] previously presented the phase diagram for the CaO-SiO_2-CaF_2 ternary system in 1966 by combining his data with Mukerji's result.[7] Based on Hillert's diagram, the present authors constructed the phase diagram of the rankinite (3CaO · $2SiO_2$)-CaF_2 system to compare with the present result, which is presented in Figure 10. His diagram is completely different from the present result due to the lack of cuspidine data. Hillert and Mukerji have described that cuspidine was not identified in their studies, and no further explanation was made on this. Actually, they did not conduct the experiments intensively on cuspidine, *i.e.*, Mukerji studied the ternary system of CaO-CaF_2-2CaO · SiO_2 and Hillert investigated the system (64 mass pct SiO_2 + 36 mass pct CaO)-CaF_2 system; therefore, they might miss

Table II. Experimental Results on the System Cuspidine-CaF_2 by Quenching Method

Sample	Initial Composition	Experimental Temperature/K	Equilibration Time /ks(h)	Liquidus Composition/Mass Pct CaO	SiO_2	CaF_2	Phases in Equilibrium at the Experimental Temperature
S1-1473-72	Sample 1	1473	259.2 (72)	—	—	—	cuspdine + CaF_2(+2CaO · SiO_2)*
S1-1623-60		1623	216 (60)	38.7	25.4	35.9	cuspidine + liquid
S1-1653-60		1653	216 (60)	—	—	—	liquid
S3-1473-72	sample 3	1473	259.2 (72)	—	—	—	cuspdine + CaF_2(+2CaO · SiO_2)*
S3-1573-72		1573	259.2 (72)	35.0	20.5	44.5	cuspdine + liquid
S3-1573-20		1573	72.0 (20)	33.4	20.5	46.0	cuspdine + liquid
S3-1573-5.8		1573	20.9 (5.8)	35.1	19.3	45.6	cuspdine + liquid
S3-1593-60		1593	216 (60)	35.0	21.3	43.7	cuspdine + liquid
S5-1473-72	sample 5	1473	259.2 (72)	—	—	—	cuspdine + CaF_2(+2CaO · SiO_2)*
S5-1493-72		1493	259.2 (72)	—	—	—	cuspdine + CaF_2(+2CaO · SiO_2)*
S5-1523-60		1523	216 (60)	—	—	—	cuspdine + CaF_2(+2CaO · SiO_2)*
S9-1473-72	sample 9	1473	259.2 (72)	—	—	—	cuspdine + CaF_2
S9-1573-72		1573	259.2 (72)	19.6	14.4	66.0	CaF_2 + liquid
S10-1623-20	sample 10	1623	72.0 (20)	16.4	12.2	71.4	CaF_2 + liquid

*Very weak XRD peaks of 2CaO · SiO_2 appeared, because the composition slightly deviated from the cuspidine-CaF_2 system and moved into the three-phase region of cuspidine-CaF_2-2CaO · SiO_2.

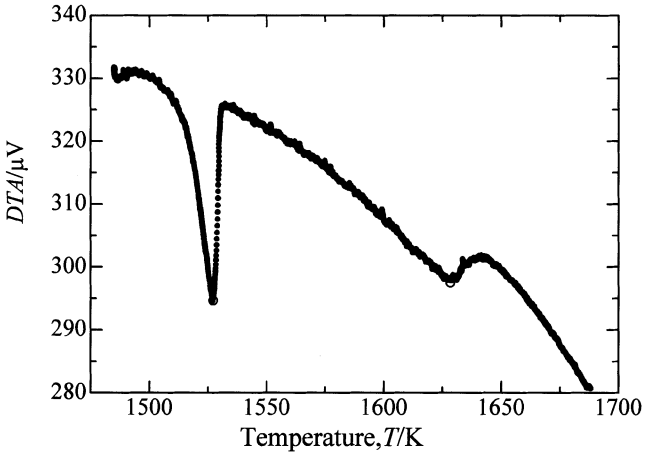

Fig. 7—DTA 19 mass pct 3CaO · $2SiO_2$ − 81 mass pct CaF_2 (sample 9) at a heating rate of 5 K/min.

Table III. Results of DTA Measurement

Initial Composition	Eutectic Temperature/K: Extrapolated Value at 0 K min^{-1}	Eutectic Temperature/K: Apparent Value (Heating Rate/K min^{-1})	Liquidus Temperature/K (Heating Rate/K min^{-1})
Sample 1		1496 (5)*	1671 (5)*
Sample 3	1516	1516 (5)	1647 (5)*
		1516 (3)	
		1516 (2)	
Sample 4	1516	1516 (5)	1575 (5)*
		1518 (3)	
		1514 (2)	
Sample 6		1515 (5)*	1576 (5)*
Sample 7	1514	1511 (5)	1543 (5)*
		1510 (5)	
		1513 (2)	
		1512 (1)	
Sample 8	1514	1521 (5)	1586 (6)*
		1517 (3)	
		1517 (2)	
Sample	1510	1516 (5)	1630 (5)*
		1514 (2)	
		1510 (1)	
Sample 10		1512 (5)*	1653 (5)*

*Calibrated by using a relation between the melting points of CaF_2 and MgF_2 and the peak temperatures obtained by DTA conducted at 5 K/min.

the presence of cuspidine. Thus, since the phase diagram for the CaO-SiO_2-CaF_2 ternary system changes significantly due to the presence of cuspidine, the ternary phase diagram, especially around cuspidine, should be established.

V. CONCLUSIONS

Equilibrium phase diagram for the system cuspidine (3CaO · $2SiO_2$ · CaF_2)-CaF_2 has been studied by the quenching method and DTA. Cuspidine congruently melts at 1680 ± 2 K. The cuspidine-CaF_2 system presents a simple eutectic type of phase diagram. The eutectic composition and temperature are 46 mass pct 3CaO · $2SiO_2$ − 54 mass pct CaF_2 and 1515 ± 3 K, respectively.

ACKNOWLEDGMENTS

This research was funded by Nippon Steel Corp., Kawasaki Steel Corp., NKK Corp., Sumitomo Metal Industries Ltd., and Kobe Steel, Ltd. This research was also supported, in part, by a grant from the Iron and Steel Institute of Japan (ISIJ research promotion grants). The authors thank Drs. T. Watanabe and M. Kawamoto, Sumitomo Metal Industries Ltd., and Dr. K. Sorimachi and Mr. A. Yamauchi, Kawasaki Steel Corp., for their valuable comments on the resent continuous casting process of steel. The authors are also grateful to Professor K.C. Mills, National Physical Laboratory, for his comments and for suggesting the reliable melting point of CaF_2.

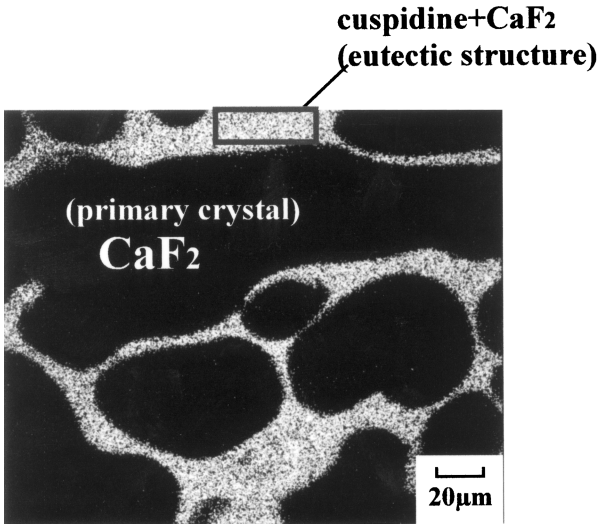

(*a*)

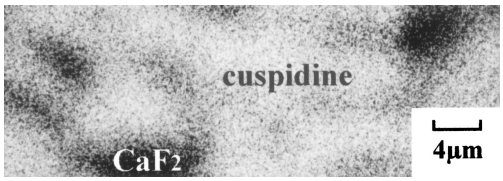

(*b*)

Fig. 8—(*a*) X-ray image of silicon of 19 mass pct $3CaO \cdot 2SiO_2$ − 81 mass pct CaF_2 (sample 9) after the DTA. (*b*) An enlarged view of the enclosed area in (a).

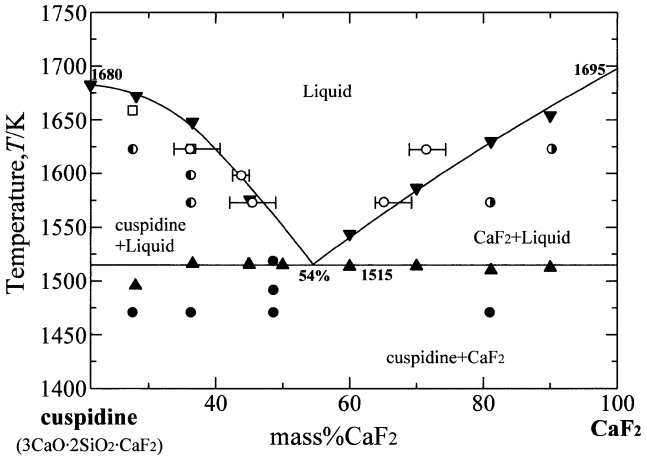

Fig. 9—Phase diagram of the system cuspidine ($3CaO \cdot 2SiO_2 \cdot CaF_2$) − CaF_2. Data from DTA are designated by triangles, and circles and squares express the results of the quenching method.

Quenching method		
Phases	Initial Composition	Liquidus Composition
Cuspidine + CaF_2	●	
Cuspidine + liquid	◐	⊢○⊣
CaF_2 + liquid	◑	
Liquid	□	

DTA	
Eutectic Temperature	Liquidus Temperature
▲	▼

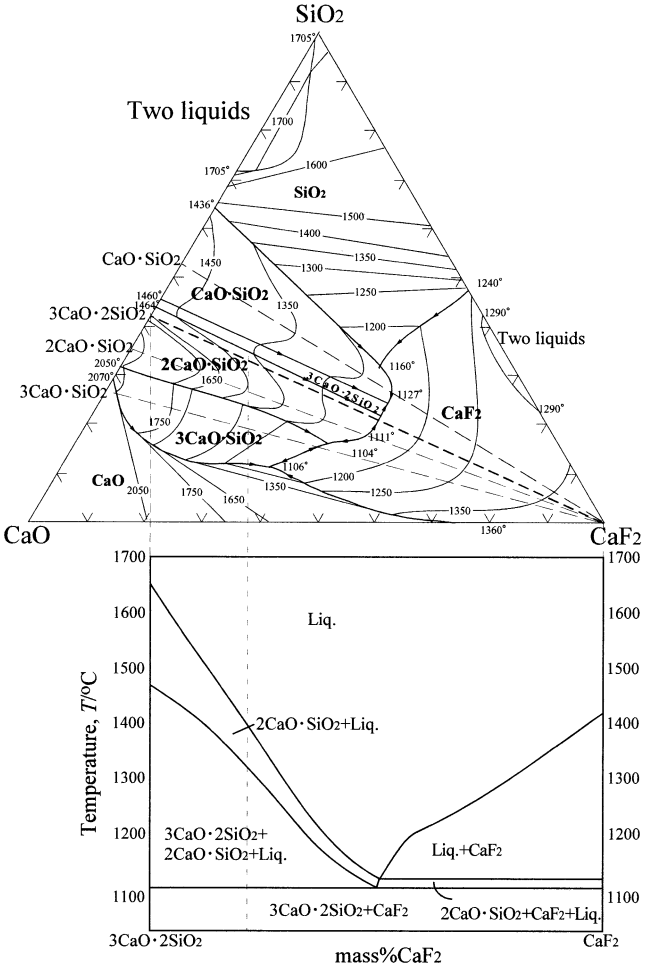

Fig. 10—Pseudobinary phase diagram of rankinite ($3CaO \cdot 2SiO_2$) − CaF_2 system constructed based on Hillert's result in mass pct.

REFERENCES

1. A. Grill and J.K. Brimacombe: *Ironmaking and Steelmaking*, 1976, vol. 3, pp. 2-76.
2. P. Grieveson, S. Bagha, N. Machingawuta, K. Liddell, and K.C. Mills: *Ironmaking and Steelmaking*, 1988, vol. 15, pp. 181-86.
3. A. Yamauchi, K. Sorimachi, T. Sakuraya, and T. Fujii: *Tetsu-to-Hagané*, 1993, vol. 79, pp. 167-74.
4. K. Watanabe, M. Suzuki, K. Murauchi, H. Kondo, A. Miyamoto, and T. Shiomi: *Tetsu-to-Hagané*, 1997, vol. 83, pp. 115-20.
5. Y. Kashiwaya, C.E. Cicutti, and A.W. Cramb: *Iron Steel Inst. Jpn. Int.*, 1998, vol. 38, pp. 357-65.
6. K. Tsutsumi J. Ohtake, T. Nagasaka, and Hino: *Tetsu-to-Hagané*, 1998, vol. 84, pp. 464-69.
7. J. Mukerji: *J. Am. Cer. Soc.*, 1965, vol. 48, pp. 210-13.
8. L. Hillert: *Acta Chemica Scandinavica*, 1966, vol. 20, pp. 290-96.
9. C. Brisi: *J. Am. Cer. Soc.*, 1957, vol. 40, pp. 174-78.
10. H. Fukuyama, T. Watanabe, M. Susa, and K. Nagata: *Proc. EPD Congr. 1999*, San Diego, CA, 1999, TMS, Warrendale, PA, 1999, pp. 61-75.
11. A. Van Valkenberg and G.F. Rynders. *Am. Mineralogist*, 1958, vol. 43, pp. 1195-1202.
12. *Rikagaku-Jiten*, 5th ed., S. Nagakura, T. Iguchi, H. Ezawa, S. Iwamura, F. Sato, eds., Iwanami-shoten Co., Tokyo, 1998, p. 1176.
13. K.C. Mills and B.J. Keene: *Int. Phys. Rev.*, 1981, vol. 1, pp. 21-69.
14. H. Suito and D.R. Gaskell: *Metall. Trans. B*, 1976, vol. 7B, pp. 559-66.
15. H. Kojima and C.R. Masson: *Can. J. Chem.*, 1969, vol. 47, pp. 4221-28.
16. Chemical Society of Japan: *Netsu-Atsuryoku, Jikken-Kagaku-Koza 4*, 4th ed., Maruzen Book Co., Tokyo, 1992, pp. 65-69.